Journal of Biomolecular NMR (2019) 73:641–650
https://doi.org/10.1007/s10858-019-00276-y

ARTICLE

Revisiting $^{1}H^{N}$ CPMG relaxation dispersion experiments: a simple modification can eliminate large artifacts

Tairan Yuwen[1] · Lewis E. Kay[1,2]

Received: 29 July 2019 / Accepted: 6 September 2019 / Published online: 23 October 2019

Abstract

Carr–Purcell–Meiboom–Gill relaxation dispersion experiments are commonly used to probe biomolecular dynamics on the millisecond timescale. The simplest experiment involves using backbone ^{15}N spins as probes of motion and pulse sequences are now available for providing accurate dispersion profiles in this case. In contrast, ^{1}H-based experiments recorded on fully protonated samples are less common because of difficulties associated with homonuclear scalar couplings that can result in transfer of magnetization between coupled spins, leading to significant artifacts. Herein we examine a version of the $^{1}H^{N}$ CPMG experiment that has been used in our laboratory where a pair of CPMG pulse trains comprising non-selective, high power ^{1}H refocusing pulses sandwich an amide selective pulse that serves to refocus scalar-coupled evolution by the end of the train. The origin of the artifacts in our original scheme is explained and a new, significantly improved sequence is presented. The utility of the new experiment is demonstrated by obtaining flat $^{1}H^{N}$ dispersion profiles in a protonated protein system that is not expected to undergo millisecond timescale dynamics, and subsequently by measuring profiles on a cavity mutant of T4 lysozyme that exchanges between a pair of distinct states, establishing that high quality data can be generated even for fully protonated samples.

Keywords Chemical exchange · $^{1}H^{N}$ CPMG · Amide protons · Fully protonated proteins · Invisible excited states · Protein dynamics

Introduction

Biological molecules can populate many different conformational states that collectively play important roles in their function (Karplus and Kuriyan 2005; Sekhar and Kay 2019). These states frequently interconvert on time-scales ranging from nano-seconds to seconds, depending on the barrier sizes that separate them (Karplus and McCammon 1983), and the ensemble of such states is often described in terms of an energy landscape (Dill and Chan 1997). An understanding of biomolecular function requires, therefore, a quantitative description of energy landscapes, including the structures that populate them, their relative stabilities and their rates of interconversion. NMR spectroscopy has played an important role in quantifying biomolecular dynamics over a wide range of timescales (Ishima and Torchia 2000; Mittermaier and Kay 2006; Palmer et al. 2001), including motions in the micro- (μs) to millisecond (ms) time-regime that are thought to be particularly critical for functional biological processes (Boehr et al. 2006; Henzler-Wildman and Kern 2007; Ishima et al. 1999; Neudecker et al. 2012; Sekhar et al. 2015, 2018). The most commonly used approaches for characterizing dynamics in the μs–ms time-window include Carr–Purcell–Meiboom–Gill (CPMG) (Palmer et al. 2001) and $R_{1\rho}$ (Palmer and Massi 2006) relaxation dispersion techniques, as well as Chemical Exchange Saturation Transfer (CEST) (Vallurupalli et al. 2017) and Dark-state Exchange Saturation Transfer (DEST) (Fawzi et al. 2011).

Electronic supplementary material The online version of this article (https://doi.org/10.1007/s10858-019-00276-y) contains supplementary material, which is available to authorized users.

✉ Lewis E. Kay
kay@pound.med.utoronto.ca

[1] Departments of Molecular Genetics, Biochemistry and Chemistry, University of Toronto, Toronto, ON M5S 1A8, Canada

[2] Program in Molecular Medicine, Hospital for Sick Children, 555 University Avenue, Toronto, ON M5G 1X8, Canada

Among a wide array of CPMG experiments for studying biomolecules, those that are based on ^{15}N-spin relaxation (Hansen et al. 2008a; Loria et al. 1999) or, in the case of isolated ^{13}C probes, ^{13}C-spin relaxation (Hansen et al. 2008b; Ishima et al. 2004; Mulder et al. 2002), are the most commonly used. ^{1}H CPMG experiments introduce challenges that arise from ^{1}H–^{1}H homonuclear scalar couplings and cross-relaxation that can lead to significant artifacts in dispersion profiles, complicating their analysis in terms of exchange parameters (Ishima and Torchia 2003; Ishima et al. 1998). Nevertheless, experiments have been designed for recording backbone amide ($^{1}H^{N}$) CPMG profiles in protonated proteins that at least minimize these effects (Ishima and Torchia 2003), while deuterium-labeling schemes, in concert with specifically designed pulse sequences that exploit the label, have been introduced for studies of ms timescale backbone ($^{1}H^{\alpha}$) and sidechain dynamics using ^{1}H probes (Hansen et al. 2012; Lundström et al. 2009). Herein we revisit the $^{1}H^{N}$-CPMG experiment, as applied to protonated samples, because our experience suggests that systematic artifacts still remain, at least in the version that we use. The major problem in such applications arises from $^{1}H^{N}$–$^{1}H^{\alpha}$ scalar-coupled evolution of transverse amide-proton magnetization during the CPMG interval. Since chemical shifts of amide and aliphatic protons are distinct, a natural idea is to apply selective 180° pulses (e.g., REBURP (Geen and Freeman 1991)) during the CPMG pulse train (Ishima and Torchia 2003). However, these require durations on the order of a ms, thereby restricting their frequency of application (ν_{CPMG}) and hence limiting rates of conformational exchange that can be explored using this strategy. An approach that we have advocated that builds upon the scheme of Ishima and Torchia while still permitting the recording of dispersion profiles with large ν_{CPMG} values is one which minimizes the effects of scalar couplings by separating high-power CPMG 180° pulses with an amide $^{1}H^{N}$ selective 180° pulse in the center of the CPMG element (Fig. S1). Such an approach was used previously in the construction of a CPMG experiment for measuring dispersion profiles of $^{1}H^{\alpha}$ protons in partially protonated protein samples (Lundström et al. 2009). As we show herein, however, artifacts still emerge. A description of the origin of these artifacts and how they can be suppressed is presented, considering both simulation and experiment. Based on this analysis a simple modification to the $^{1}H^{N}$ CPMG pulse sequence is introduced that leads to flat dispersion profiles in the absence of chemical exchange, in many cases approaching the quality of $^{1}H^{N}$ CPMG curves recorded on highly deuterated protein samples. The modified pulse scheme is then used to study chemical exchange in a protonated sample of the L99A cavity mutant of T4 lysozyme from bacteriophage (L99A T4L) (Eriksson et al. 1992) where it is shown that an improved quality of fit is obtained relative to that generated from analysis of data recorded with the original experiment. Robust estimates of exchange parameters and chemical shifts are readily obtained using the new experiment.

Materials and methods

Sample preparation

Samples of the B1 domain of peptostreptococcal protein L (referred to as protein L in what follows) were prepared as described previously (Bouvignies and Kay 2012; Mittermaier and Kay 2001). Protein concentrations were 4.0 mM or 1.0 mM for [U-^{2}H,^{15}N]- or [U-^{15}N]-labeled samples, respectively, dissolved in 50 mM sodium phosphate, 0.05% NaN_3, 90% H_2O/10% D_2O, pH 6.0. T4 lysozyme samples containing the L99A cavity mutant were generated by following the protocol described by Bouvignies et al. (Bouvignies et al. 2011). Protein concentrations were 1.5 mM or 1.0 mM for [U-^{2}H,^{15}N] or [U-^{15}N]-labeled samples, respectively, dissolved in 50 mM sodium phosphate, 25 mM NaCl, 2 mM EDTA, 2 mM NaN_3, pH 5.5, 90% H_2O/10% D_2O.

NMR spectroscopy

All NMR experiments were performed using Bruker AVANCE III 600 and 800 MHz spectrometers equipped with cryogenically cooled probes with triple-axis pulsed field gradients. Experiments were carried out at 800 MHz for protein L and at both fields for L99A T4L. ^{15}N CPMG datasets were recorded using a slightly improved version of the pulse scheme of Yang and coworkers (Jiang et al. 2015), modified to account for both longitudinal and transverse relaxation during the CPMG pulses. $^{1}H^{N}$ CPMG experiments using our previous scheme that included a central REBURP pulse (Fig. S1) or the new approach employing EBURP pulses (Geen and Freeman 1991) (see text) were recorded with CPMG pulses phase cycled as [0013] to achieve better off-resonance refocusing (Yip and Zuiderweg 2004). $^{1}H^{N}$ CPMG datasets were recorded using a constant-time CPMG element (Mulder et al. 2001; Tollinger et al. 2001) with T_{relax} = 20 ms. Experiments were recorded as pseudo-3D datasets by varying the number, N, of CPMG pulses during the T_{relax} interval (1 N value for each 2D plane). A series of 2D maps were obtained with ν_{CPMG} values varying between 50 Hz and 2000 Hz (protein L) or 50–1000 Hz (L99A T4L). Additional experiments were carried out on the fully protonated protein L sample using T_{relax} = 10 ms and ν_{CPMG} varying between 200–5000 Hz. Twenty to thirty planes were recorded for

each dispersion series, including duplicates for error analysis (Korzhnev et al. 2004b). The total measurement time for each experiment at each magnetic field was ~11 h (protein L) or ~22 h (L99A T4L).

Data analysis

All NMR spectra were processed and analyzed using the *NMRPipe* suite of programs (Delaglio et al. 1995) with peak intensities extracted with the *autofit* subroutine. Effective transverse relaxation rates, $R_{2,eff}$, were calculated based on peak intensities according to the relation $R_{2,eff}(\nu_{CPMG}) = -\ln(I(\nu_{CPMG})/I_0)/T_{relax}$, where I_0 is the peak intensity in a reference spectrum recorded without the relaxation delay, T_{relax} (Mulder et al. 2001). Fitting of cross-peaks in CPMG datasets was carried out using the software package *ChemEx* (https://github.com/gbouvignies/ChemEx). Only residues with dispersion profiles such that $R_{ex} = R_{2,eff}(\nu_{CPMG} = 50\ \text{Hz}) - R_{2,eff}(\nu_{CPMG} = 1000\ \text{Hz}) > 2\ \text{s}^{-1}$ at 800 MHz were included in the CPMG data analysis. Exchange parameters were extracted from fits of dispersion data to a two-state exchange model using the Bloch–McConnell equations (McConnell 1958) assuming that the difference in transverse relaxation rates of corresponding spins in the ground and excited states, ΔR_2, is 0 s^{-1} (i.e., $R_{2,E} = R_{2,G}$).

Results and discussion

Origin of artifacts in $^1H^N$ CPMG profiles recorded on protonated protein samples

A limitation of ^{1}H CPMG-based experiments for quantifying exchange dynamics in biomolecules is that the method is sensitive to homonuclear scalar couplings, often leading to significant fluctuations in dispersion profiles that reflect the nature of the coupled spin system and to rates of magnetization transfer between the scalar-coupled spins that vary with ν_{CPMG} ($\nu_{CPMG} = 1/(2\delta)$ where δ is the delay between successive 180° refocusing pulses) (Bouvignies et al. 2014; Ishima and Torchia 2003; Lundström et al. 2009). In the specific context of $^1H^N$ CPMG experiments recorded on protonated protein samples $^1H^N$–$^1H^\alpha$ scalar couplings are particularly deleterious, introducing artifacts in dispersion curves (Ishima and Torchia 2003). For this reason, it is highly advantageous to prepare ^{2}H-samples for such studies, yet in some cases the cost can be prohibitive, or perhaps a protonated sample is already available and preliminary experiments can be obtained on it to assess the system for further in-depth analysis with optimal samples. With this in mind we have revisited our experiment with a goal of improving the quality of the resulting profiles.

Figure 1 (top) illustrates the basic pulse scheme that we have used in the past to record $^1H^N$ CPMG experiments on protonated proteins (see Fig. S1 for the full sequence), where the black rectangular pulses are applied with high power (typically 25 kHz field) and the central (REBURP) pulse is selective for the amide proton region of the spectrum. In this way any scalar-coupled evolution of magnetization during the first half of the CPMG element via $^3J_{\text{HNH}\alpha}$ would be expected, at least partially, to be refocused in the second half, thereby minimizing the effects of the coupling. Yet, large artifacts still remain in protein applications, as can be seen in Fig. 1a, b where a pair of profiles are shown for residues N7 and E19, measured in fully protonated (red) or perdeuterated (green) samples of protein L. We have not been able to detect exchange in most residues of this domain from 'clean' CPMG datasets, such as those obtained from ^{15}N relaxation dispersion, or $^1H^N$ relaxation dispersion when recorded on highly deuterated preparations (Fig. 1a, b green).

To understand how the artifacts observed for the protonated sample arise we turned to simulations, using a simple three-spin system that included $^1H^N$, $^1H^\alpha$ and $^1H^\beta$ spins with $^3J_{\text{HNH}\alpha} = 10$ Hz, $^4J_{\text{HNH}\beta} = 2$ Hz, and $^3J_{\text{H}\alpha\text{H}\beta} = 10$ Hz, Fig. 1c. A REBURP pulse of duration 1.52 ms was considered (4.1 kHz B_1 field) that refocuses over a bandwidth of 4 ppm for an 800 MHz spectrometer, and the pulses in the CPMG trains were applied with a 25 kHz field, as in experiments. Notably, large differences in dispersion curves were obtained for different offsets of the $^1H^\alpha$ spin, and only for $\delta_{\text{H}\alpha} = 4.4$ ppm was the expected flat profile generated. The origin of the problem can be appreciated by the realization that pulse imperfections (off-resonance effects and miscalibrations) result in the generation of transverse $^1H^\alpha$ magnetization via a transfer pathway that can be cogently described as follows

$$H_X^N \xrightarrow{^3J_{\text{HNH}\alpha}} 2H_Y^N H_Z^\alpha \xrightarrow{\text{ImperfectPulsesinCPMGTrain}} 2H_Y^N H_Z^\alpha, 2H_Y^N H_Y^\alpha, 2H_Y^N H_X^\alpha \ldots \quad (1)$$

where L_j is the $j \in \{X, Y, Z\}$ component of magnetization (see below). The transverse $^1H^\alpha$ magnetization so generated evolves during the REBURP selective pulse that is centered in the middle of the amide proton region (for the simulation at 8.2 ppm) and this chemical shift evolution is not refocused, leading to the observed oscillations in peak intensities as a function of ν_{CPMG}. For a given REBURP pulse length and corresponding RF power there will be an $^1H^\alpha$ offset such that the transverse magnetization is completely refocused, 4.4 ppm in the example of Fig. 1, and in this case artifact-free profiles are simulated.

The simulations of Fig. 1 establish that evolution of 'aberrant' transverse $^1H^\alpha$ magnetization during the central pulse element must be refocused if flat profiles are to be

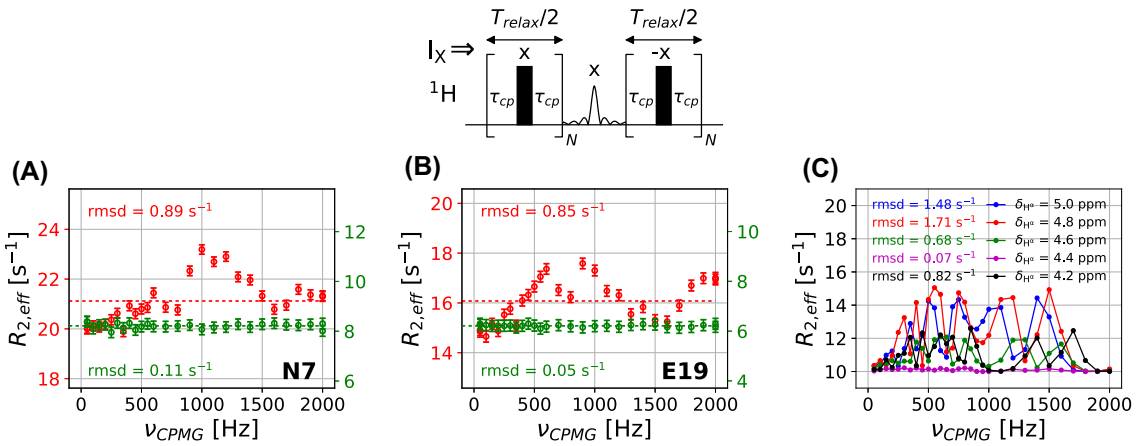

Fig. 1 **a** and **b** $^1H^N$ CPMG dispersion profiles measured on perdeuterated (green) and fully protonated (red) protein L samples using the pulse scheme of Fig. S1, 800 MHz, 25 °C; the CPMG element that includes a central, amide proton selective REBURP pulse is shown and the initial magnetization is along the x-axis. Large artifacts are produced for the fully protonated sample. **c** shows results from numerical simulations carried out for a three-spin system, $\{^1H^N, ^1H^\alpha, ^1H^\beta\}$, that does not include chemical exchange, using the pulse scheme illustrated. Values of T_{relax} = 20 ms and ν_1 = 25 kHz were used for all simulations, that assumed a ^1H resonance frequency of 800 MHz. Scalar couplings of $^3J_{HNH\alpha}$ = 10 Hz, $^4J_{HNH\beta}$ = 2 Hz and $^3J_{H\alpha H\beta}$ = 10 Hz were used, and the full $^1H^N$–$^1H^\alpha$ scalar-coupled Hamiltonian was considered in each simulation. The ^1H RF carrier was positioned at 8.2 ppm, with $^1H^N$ and $^1H^\beta$ chemical shifts set to 8.2 ppm and 2.0 ppm respectively, and the chemical shift of the $^1H^\alpha$ spin for each simulation is indicated in the panel. The excitation bandwidth for the REBURP pulse is 4.0 ppm (1.52 ms, maximum B_1 field of 4.1 kHz). The intrinsic $^1H^N$ relaxation rates were set to R_1 = 2 s^{-1}, R_2 = 10 s^{-1}, and differential relaxation between in-phase and anti-phase $^1H^N$ magnetization was not considered, with relaxation rates of MQ coherences set to R_2

obtained in the absence of chemical exchange. As a first step towards developing a pulse scheme that could achieve this goal we considered two CPMG sequences, illustrated in Fig. 2a, b, where the amide proton selective pulse (hatched pulse) was assumed, for the purposes of simulation, to be a 'perfect' pulse and of 0 s duration. In the first case, Fig. 2a, the two halves of the CPMG train comprise pulses of phase x and −x, that, in principle, should self-compensate for imperfections (Hansen et al. 2008a). In the second case, Fig. 2b, the selective pulse is applied along the y-axis, orthogonal to the phases of the CPMG pulses (all along x) that should yield equivalent compensation for pulse imperfections as the initial scheme (Fig. 2a), at least for isolated spin-1/2 spin systems or for heteronuclear two-spin spin-systems. Yet very different CPMG profiles are observed, with the sequence of Fig. 2a clearly superior.

In an effort to understand the differences we consider a homonuclear I–S two-spin system where $I = ^1H^N$ and

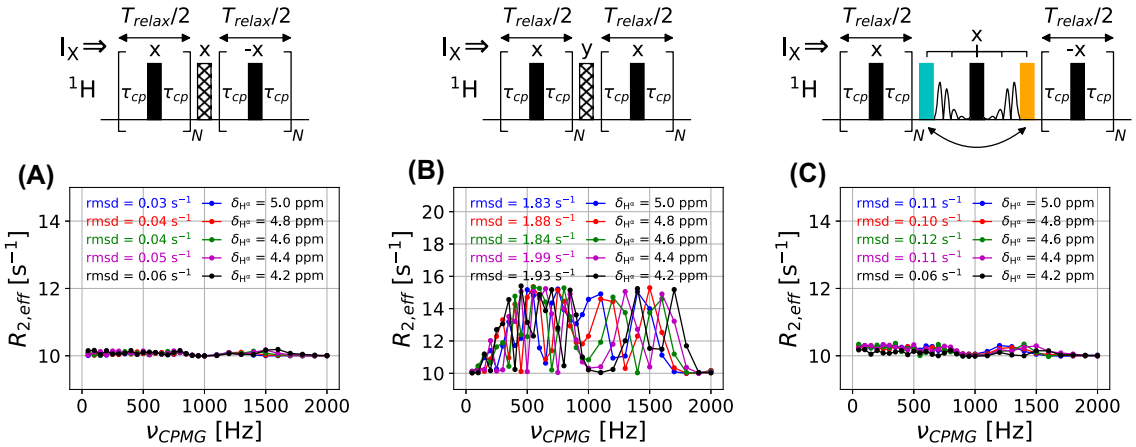

Fig. 2 Simulated $^1H^N$ CPMG dispersion profiles with initial $^1H^N$ magnetization along the x-axis. Pulse schemes used in the simulations are indicated above each of the panels. The central pulse (infinitely short, represented by a hatched bar) in the schemes above panels **a** and **b** is assumed to generate an ideal, selective 180° rotation on $^1H^N$ magnetization, while the remaining rectangular pulses are applied with a 25 kHz field. Simulations in panel **c** use central amide-selective EBURP pulses of duration 1.4 ms (2.8 kHz B_1 field). All simulations assumed a ^1H resonance frequency of 800 MHz and were performed using the same parameters as in the legend to Fig. 1. Both odd and even values of N are considered in the simulations

$S = {}^1H^{\alpha}$, respectively, and assume an ideal 180° selective pulse of zero width applied on spin I in the center of the pulse train. Then the schemes of Fig. 2a, b are given by the propagators $\hat{P}_2 \exp(-i\pi\hat{I}_X)\hat{P}_1$ and $\hat{P}_1 \exp(-i\pi\hat{I}_Y)\hat{P}_1$ respectively, where

$$\begin{aligned}\hat{P}_1 = &\{\exp\left(-i\left(\omega_I\hat{I}_Z + \omega_S\hat{S}_Z + 2\pi J_{IS}\hat{I}_Z\hat{S}_Z\right)\tau_{cp}\right)\\ &\exp\left(-i\left(\omega_1\hat{I}_X + \omega_I\hat{I}_Z + \omega_1\hat{S}_X + \omega_S\hat{S}_Z + 2\pi J_{IS}\hat{I}_Z\hat{S}_Z\right)\tau_p\right)\\ &\exp\left(-i\left(\omega_I\hat{I}_Z + \omega_S\hat{S}_Z + 2\pi J_{IS}\hat{I}_Z\hat{S}_Z\right)\tau_{cp}\right)\}^N\\ \hat{P}_2 = &\{\exp\left(-i\left(\omega_I\hat{I}_Z + \omega_S\hat{S}_Z + 2\pi J_{IS}\hat{I}_Z\hat{S}_Z\right)\tau_{cp}\right)\\ &\exp\left(-i\left(-\omega_1\hat{I}_X + \omega_I\hat{I}_Z - \omega_1\hat{S}_X + \omega_S\hat{S}_Z + 2\pi J_{IS}\hat{I}_Z\hat{S}_Z\right)\tau_p\right)\\ &\exp\left(-i\left(\omega_I\hat{I}_Z + \omega_S\hat{S}_Z + 2\pi J_{IS}\hat{I}_Z\hat{S}_Z\right)\tau_{cp}\right)\}^N\end{aligned} \tag{2}$$

In Eq. (2) ω_I and ω_S are the chemical shifts of spins I and S, respectively, ω_1 is the RF field strength of the CPMG pulses, and, for simplicity, only the Hamiltonian for weak I–S coupling is considered ($|\omega_I - \omega_S| \gg 2\pi J_{IS}$), although in all simulations the complete form of the scalar-coupled Hamiltonian was used. The effect of the central 180° pulse can be regarded as modifying the propagator for the second half of the CPMG pulse train as follows

$$\begin{aligned}\hat{P}'_2 = &\exp(i\pi\hat{I}_X)\hat{P}_2\exp(-i\pi\hat{I}_X) = \{\exp\left(i\left(\omega_I\hat{I}_Z - \omega_S\hat{S}_Z + 2\pi J_{IS}\hat{I}_Z\hat{S}_Z\right)\tau_{cp}\right)\\ &\exp\left(i\left(\omega_1\hat{I}_X + \omega_I\hat{I}_Z + \omega_1\hat{S}_X - \omega_S\hat{S}_Z + 2\pi J_{IS}\hat{I}_Z\hat{S}_Z\right)\tau_p\right)\\ &\exp\left(i\left(\omega_I\hat{I}_Z - \omega_S\hat{S}_Z + 2\pi J_{IS}\hat{I}_Z\hat{S}_Z\right)\tau_{cp}\right)\}^N\\ \hat{P}'_1 = &\exp(i\pi\hat{I}_Y)\hat{P}_1\exp(-i\pi\hat{I}_Y) = \{\exp(i(\omega_I\hat{I}_Z - \omega_S\hat{S}_Z + 2\pi J_{IS}\hat{I}_Z\hat{S}_Z)\tau_{cp})\\ &\exp(i(\omega_1\hat{I}_X + \omega_I\hat{I}_Z - \omega_1\hat{S}_X - \omega_S\hat{S}_Z + 2\pi J_{IS}\hat{I}_Z\hat{S}_Z)\tau_p)\\ &\exp(i(\omega_I\hat{I}_Z - \omega_S\hat{S}_Z + 2\pi J_{IS}\hat{I}_Z\hat{S}_Z)\tau_{cp})\}^N\end{aligned} \tag{3}$$

Perfect refocusing of scalar-coupled evolution with either of schemes A or B would require that $\hat{P}_2 \exp(-i\pi\hat{I}_X)\hat{P}_1 = \exp(-i\pi\hat{I}_X)$ or $\hat{P}_1 \exp(-i\pi\hat{I}_Y)\hat{P}_1 = \exp(-i\pi\hat{I}_Y)$, corresponding to $\hat{P}'_2\hat{P}_1 = \hat{1}$ or $\hat{P}'_1\hat{P}_1 = \hat{1}$, respectively, where $\hat{1}$ is the identity operator. This is not possible in the case of a homonuclear scalar-coupled two-spin system where the CPMG pulses are non-selective, since in the general case neither $\hat{P}'_2$ nor $\hat{P}'_1$ equals $\hat{P}_1^{-1}$, where

$$\begin{aligned}\hat{P}_1^{-1} = &\{\exp(i(\omega_I\hat{I}_Z + \omega_S\hat{S}_Z + 2\pi J_{IS}\hat{I}_Z\hat{S}_Z)\tau_{cp})\\ &\exp(i(\omega_1\hat{I}_X + \omega_I\hat{I}_Z + \omega_1\hat{S}_X + \omega_S\hat{S}_Z + 2\pi J_{IS}\hat{I}_Z\hat{S}_Z)\tau_p)\\ &\exp(i(\omega_I\hat{I}_Z + \omega_S\hat{S}_Z + 2\pi J_{IS}\hat{I}_Z\hat{S}_Z)\tau_{cp})\}^N\end{aligned} \tag{4}$$

Yet it appears from the simulated profiles in Fig. 2a, b that $\hat{P}'_2$ more closely approximates $\hat{P}_1^{-1}$ than does $\hat{P}'_1$, as the artifacts are much smaller in Fig. 2a. That this is, in fact, the case can be made clear by simulating the evolution of an I–S homonuclear two-spin system, starting with initial magnetization along x (i.e., I_X) and considering all 16 terms that can be created during the course of the CPMG pulse train (Dittmer and Bodenhausen 2006). In Fig. S2 we have evaluated each of the density elements, $\hat{O}$, at the end of a CPMG train according to $\hat{P}'_2\hat{O}(\hat{P}'_2)^{-1}$ and $\hat{P}'_1\hat{O}(\hat{P}'_1)^{-1}$ and compared the results with $(\hat{P}_1)^{-1}\hat{O}\hat{P}_1$. Notably, only a number of the terms show appreciable magnitudes, including the starting element I_X and the anti-phase component $2I_YS_Z$ that evolves from ${}^3J_{\mathrm{HNH}\alpha}$, as well as the double- and zero-quantum terms $2I_YS_X$ and $2I_YS_Y$. Of the two multiple quantum terms, the magnitude of $2I_YS_Y$ is considerably larger after the N echoes of a CPMG train are completed (Fig. S2), and $\hat{P}'_2\hat{O}(\hat{P}'_2)^{-1} \approx (\hat{P}_1)^{-1}\hat{O}\hat{P}_1$ in this case. This implies that scheme A, $\hat{P}_2 \exp(-i\pi\hat{I}_X)\hat{P}_1$, is preferred for the ${}^1H^N$–${}^1H^{\alpha}$ spin system that is relevant to the problem in hand. Further simulations establish that the artifact level decreases with increasing ${}^1H$ B_1 strength used for the CPMG pulses; typically we use 25 kHz fields in our experiments.

Having established the importance of ensuring that there is no chemical shift evolution for ${}^1H^{\alpha}$ spins during the central pulse element and that there is an important phase relation between the CPMG pulses and the selective ${}^1H^N$ pulse in the middle of the pulse train we developed a simple scheme that satisfies these criteria, as illustrated in Fig. 2c. All rectangular pulses are non-selective, with either the cyan or orange pulse applied alternately in each scan and the shaped pulses are of the EBURP variety (Geen and Freeman 1991), centered in the amide proton region. The net effect of this element is to act as a selective pulse on the ${}^1H^N$ spins, while leaving the ${}^1H^{\alpha}$ spins unperturbed. Note that the symmetric positioning of the pair of EBURP pulses about the central (black) ${}^1H$ 180° ensures that there is no net chemical shift evolution for the ${}^1H^{\alpha}$ spins. Figure 2c presents a series of dispersions profiles that have been simulated with this scheme, as a function of ${}^1H^{\alpha}$ resonance position in the absence of chemical exchange, showing that the profiles are of high quality (i.e., flat) for the proposed scheme.

Figure 3 presents the full ${}^1H^N$ CPMG based experiment that we have developed for studies involving protonated proteins. It is worth noting that, as in the schemes of Figs. 1 and 2, a divided CPMG element is used, consisting of a pair of pulse trains $[\tau_{cp}-180^{\circ}_{\psi}-\tau_{cp}]_N$ that are separated by a scheme that selectively refocuses amide protons while leaving the ${}^1H^{\alpha}$ spins unaffected. It is important to emphasize that such a scheme, in which a total of $2N$ CPMG pulses are applied, refocuses errors in CPMG pulses for both even and odd N, as we have discussed in detail previously (Hansen et al. 2008a) and demonstrated experimentally for a number of different CPMG experiments including those using either ${}^{15}N$ or ${}^{13}C$ probes of exchange (Korzhnev et al. 2004a; Vallurupalli et al. 2007).

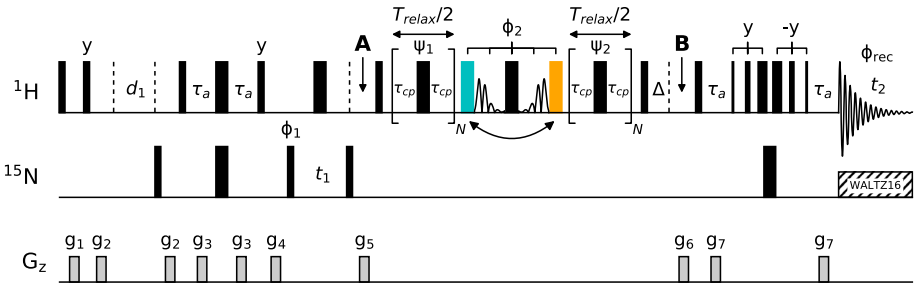

Fig. 3 Pulse sequence of the $^1H^N$ CPMG experiment for studies of fully protonated proteins. All 90° (180°) rectangular pulses are denoted by narrow (wide) bars. These are applied at maximum power, with exception of the ^{1}H pulses during the CPMG element (pulses of phase ϕ_2, ψ_1, and ψ_2) that use a ~25 kHz field. Both EBURP and time-reversed EBURP pulses are shown with their actual shapes, covering the amide $^1H^N$ region. Typically these pulses have durations of ~1.4 ms (800 MHz field, 2.8 kHz B_1 field strength, 4.0 ppm excitation bandwidth). All pulses are applied along x unless otherwise indicated. The ^{1}H carrier is placed in the center of the amide proton spectrum (~8.2 ppm) during the interval indicated between *A* and *B*, and positioned at the water resonance (~4.7 ppm) at other times. Cyan/orange pulses are alternatingly applied in every two scans. The ^{15}N carrier is placed in the center of the amide region (~119 ppm) and ^{15}N WALTZ-16 decoupling (Shaka et al. 1983) is applied during acquisition (t_2). The delays used are: τ_a = 2.38 ms, $\tau_{cp} = T_{relax}/(4N) - \text{pwh}_{180} \times 0.5 \times 0.75$ where pwh_{180} is the length of each refocusing CPMG pulse (see pulse sequence code) and the delay time $\Delta = (N_{max} - N) \times \text{pwh}_{180} \times 0.5$ compensates for longitudinal relaxation of $^1H^N$ magnetization during the CPMG pulses. The phase cycle is ϕ_1 = x, −x, −x, x, −x, x, x, −x; ϕ_2 = 4(y), 4(−y), 4(−y), 4(y); ϕ_{rec} = x, −x, −x, x, −x, x, x, −x. A minimum phase cycle of 2 steps is required. The phases ψ_1/ψ_2 are used to implement the [0013] scheme (Yip and Zuiderweg 2004) that is applied to the CPMG pulses. Phase ψ_1 is incremented with the cycle (y, y, −x, x) for each successive pulse, such that if N = 3 the phases of the first, second and third pulses of the first CPMG train are y, y and −x, respectively, and ψ_2 is decremented starting from the final ψ_1 phase with y and −y interchanged, such that the phases of the first, second and third pulses in the second train are −x, −y and −y, respectively (Yuwen et al. 2016, 2019). Quadrature detection in F_1 is achieved by STATES–TPPI of ϕ_1 (Marion et al. 1989). A 3-9-19 WATERGATE element (Sklenar et al. 1993) is applied prior to t_2 acquisition for water suppression. Gradients are applied with the following durations (ms) and strengths (in % maximum): g_1: (1.0, 7.5%), g_2: (1.0, 15%), g_3: (0.5, 20%), g_4: (1.0, 30%), g_5: (0.8, –50%), g_6: (1.0, 40%), g_7: (0.8, 80%)

This is in contrast to other implementations of dispersion experiments, such as those of the relaxation compensation variety (Loria et al. 1999), where N must be even (Hansen et al. 2008a). Thus, in the present implementation where the value of N is not restricted, the smallest ν_{CPMG} value can be half as large as would otherwise be the case, allowing studies of more slowly exchanging systems. In the development of the sequence we have followed the suggestion of Ishima and Torchia whereby the CPMG pulse train is placed after the ^{15}N t_1 evolution period that minimizes the effects of $^1H^N$–$^1H^N$ cross relaxation during rapid CPMG pulsing, effectively ensuring that amide proton spins relax as 'unlike spins' that increases the relaxation times of the amide protons (Ishima and Torchia 2003; Ishima et al. 1998). In order to improve the off-resonance performance of the pulse train a [0013] phase cycle has been used (Jiang et al. 2015; Yip and Zuiderweg 2004; Yuwen and Skrynnikov 2014), the τ_{cp} delays have been adjusted for the length of the CPMG pulses and an additional delay inserted after the CPMG period (Δ in Fig. 3) to compensate for longitudinal relaxation during the pulse train (see legend to Fig. 3 for details). In this way flat dispersion profiles (in the absence of exchange) can be obtained without ν_{CPMG}-dependent corrections that are typically required in other implementations of the [0013] phase cycle (Jiang et al. 2015).

Critical to the experiment is the amide proton selective pulse in the center of the CPMG interval. Since each of the two EBURP pulses has a similar duration as a REBURP pulse (assuming the same excitation bandwidth), the overall length of the pulse sequence becomes slightly longer, that may cause a small signal loss compared with the REBURP scheme (compare Figs. 3 and S1). In order to achieve optimal suppression of $^1H^N$–$^1H^\alpha$ scalar couplings the excitation bandwidth of the EBURP pulses must be chosen with care, ensuring that the amide $^1H^N$ protons are refocused while the aliphatic $^1H^\alpha$ spins are not excited. In general, we recommend that the upfield limit of the EBURP pulse excitation range be set to approximately 6.5 ppm. Figure S3 shows the results from simulations where evolution from $^1H^N$–$^1H^\alpha$ couplings are not fully refocused in cases where the RF carrier is positioned at 8.2 ppm and a 4 ppm excitation bandwidth is used for the EBURP pulses. Note that for these settings spurious $^1H^N$ dispersion profiles can be obtained when the coupled $^1H^\alpha$ spins have downfield resonance positions or amide protons have upfield chemical shifts.

Experimental verification

The performance of the pulse sequence of Fig. 3 was tested experimentally using a sample of protein L, a small domain for which millisecond timescale exchange dynamics are

almost completely absent. As a baseline we first recorded $^{1}H^{N}$ CPMG profiles on a perdeuterated sample, avoiding the problems associated with homonuclear scalar couplings altogether. Flat profiles were obtained for the great majority of residues (several show small dispersions) that could be fitted by horizontal lines with an rmsd of 0.10 ± 0.04 s^{-1} (56 residues). Experiments were subsequently recorded on a fully protonated protein L sample. Horizontal-line fits of the resulting profiles measured with the REBURP (Fig. S1) and EBURP (Fig. 3) schemes produced rmsd values of 0.35 ± 0.21 s^{-1} and 0.20 ± 0.07 s^{-1}, respectively. Nearly identical signal-to-noise ratios are obtained in spectra recorded with either sequence due to the relatively small molecular weight of this domain (6.9 kDa). Figure 4 shows selected dispersion profiles recorded on protonated (blue, red) and perdeuterated (green) protein L samples, 800 MHz, 25 °C. Although using a central REBURP refocusing pulse is problematic (red), flat profiles are obtained when EBURP pulses are used, and of course when a perdeuterated sample is employed. The offset of green and blue curves reflects the slower $^{1}H^{N}$ transverse relaxation rates for the deuterated sample. In applications involving small proteins, such as protein L that is used as a test sample here, we see similar results for experiments that utilize either [0013] or [0000] phase cycles for the CPMG pulses, Fig. S4, although for studies of larger proteins with a significant imbalance between R_1 and R_2 relaxation rates the improvement in performance with the [0013] scheme becomes obvious, Fig. S5.

It is worth noting that the sequence of Fig. 3 does not contain a 'P-element' (Loria et al. 1999). Such a module is often utilized in CPMG pulse schemes, in particular those focusing on heteronuclear probes such as ^{15}N or ^{13}C, to ensure that the average relaxation during the CPMG pulse train is independent of ν_{CPMG}. The flat profiles we obtain for protein L suggest that differential relaxation between in-phase (IP) and anti-phase (AP) $^{1}H^{N}$ magnetization is small. To verify this we have measured Δ (= $R_{2,IP} - R_{2,AP}$) for $^{1}H^{N}$ magnetization using the pulse schemes of Fig. S6, ν_{CPMG} = 2000 Hz, 800 MHz, with $\Delta = 0.29 \pm 0.57$ s^{-1} obtained. Values of Δ are related to ^{15}N R_1 rates and decrease as a function of increasing protein size and static magnetic field.

We have also performed an additional experiment on the fully protonated protein L sample using a higher range of ν_{CPMG} values (Fig. S7). Notably, small rmsds were observed suggesting that the $^{1}H^{N}$ CPMG experiment of Fig. 3 is suitable for studying sub-ms protein dynamics, which is usually difficult to achieve using other spin probes such as ^{15}N. Importantly, the [0013] scheme induces little Hartmann–Hahn transfer between $^{1}H^{N}$ and $^{1}H^{\alpha}$ spins even for ν_{CPMG} values around 5 kHz, Fig. S8.

Having shown that the artifact level of the EBURP-based $^{1}H^{N}$ CPMG experiment is much lower than our previous version that utilized a central REBURP pulse we next carried out experiments on a cavity mutant of T4

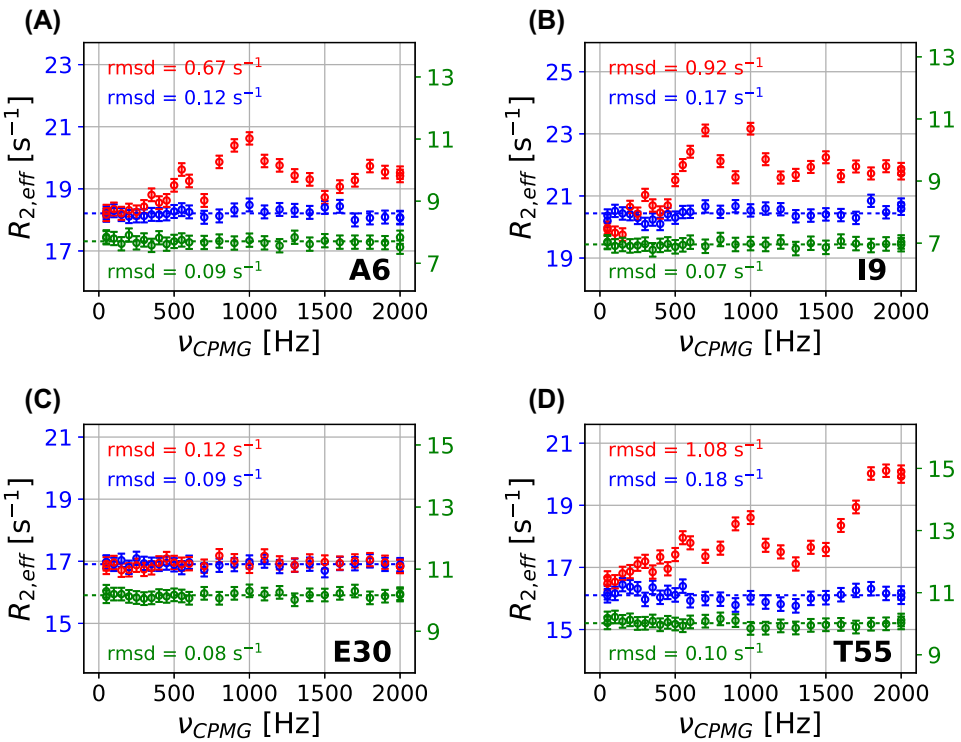

Fig. 4 Selected $^{1}H^{N}$ CPMG dispersion profiles recorded on perdeuterated (green) or fully protonated protein L samples, 800 MHz, 25 °C, using EBURP (Fig. 3, blue) or REBURP (Fig. S1, red) schemes. Essentially identical results are obtained from either experimental approach when perdeuterated samples are used. The rmsd for each dispersion profile is shown in each panel, color-coded as the dispersion. Note that there is no compensation for differential relaxation between in-phase and anti-phase $^{1}H^{N}$ magnetization in our pulse schemes, but these effects are small (see text)

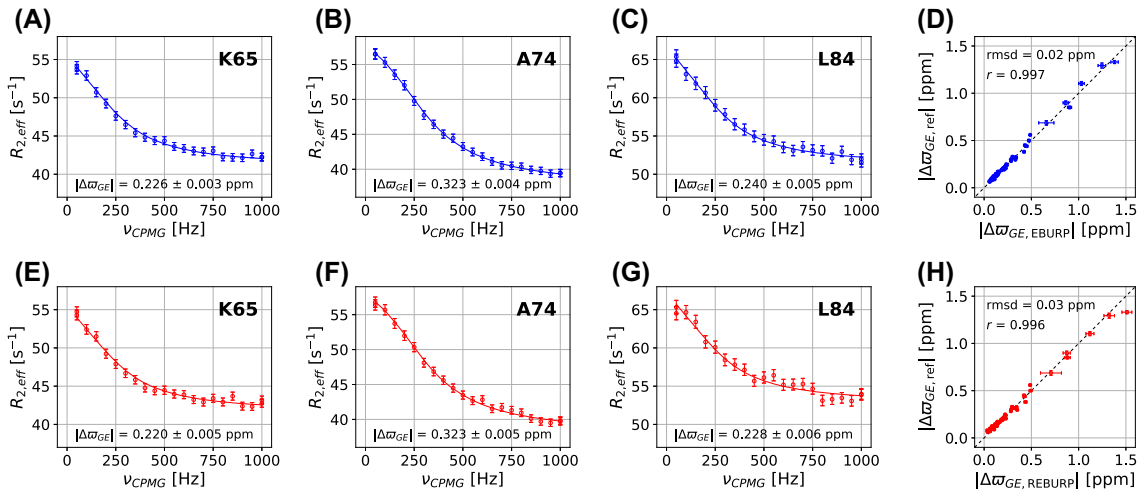

Fig. 5 Selected $^{1}H^{N}$ CPMG dispersion profiles recorded on a fully protonated sample of L99A T4L, 800 MHz, 25 °C, using either EBURP- (blue, panels **a**–**c**) or REBURP- (red, panels **e**–**g**) based pulse schemes. Correlation of $|\Delta\varpi_{GE}|$ values (56 residues) obtained from fits of data sets measured on fully protonated (x-axis) or perdeuterated (y-axis) samples is shown in panels **d** and **h**. Profiles were measured with pulse schemes of Figs. 3 or S1

lysozyme in which a leucine at position 99 is replaced by an alanine, referred to as L99A T4L in what follows (Eriksson et al. 1992). We have previously shown that large exchange profiles are observed that report on a conformational equilibrium in which Phe 114 is projected into the cavity in a minor conformer (Bouvignies et al. 2011). Dispersion profiles, using pulse schemes of Figs. 3 and S1, have been recorded on a fully protonated L99A T4L sample, with a selected subset of them shown in Fig. 5. High quality data are obtained using either approach (compare blue and red profiles) since dispersions are large and artifacts from the central REBURP pulse are considerably smaller, typically on the order of 1–2 s^{-1}. It is not surprising, therefore, that the differences in $^{1}H^{N}$ chemical shifts between ground and excited states, $|\Delta\varpi_{GE}|$, as measured using either experiment are in good agreement with values measured on the perdeuterated sample. The exchange parameters (p_E, k_{ex}) corresponding to the fraction of the sparsely populated, invisible state and the exchange rate between the two interconverting states are ($2.60 \pm 0.02\%$, $1217 \pm 16\ s^{-1}$) and ($2.56 \pm 0.03\%$, $1223 \pm 23\ s^{-1}$) for the EBURP and REBURP schemes, respectively (56 residues), while (p_E, k_{ex}) = ($2.63 \pm 0.03\%$, $1247 \pm 9\ s^{-1}$) is obtained from analysis of ^{15}N CPMG dispersion data (46 residues), Fig. 6. Notably, a lower reduced χ^2 is obtained when fitting the EBURP dataset relative to the corresponding REBURP profiles that reflects the smaller 'artifact content' of the data in the former case. Finally, the signal-to-noise is ~7% lower for the EBURP scheme on average; the slight decrease in sensitivity is expected for a molecule tumbling with a correlation time of 11 ns (Skrynnikov et al. 2001). None of the analyses considered above took into account differential relaxation between in-phase and anti-phase amide $^{1}H^{N}$ magnetization which was measured to be $0.89 \pm 1.90\ s^{-1}$ and $0.29 \pm 1.89\ s^{-1}$ at 600 and 800 MHz, respectively (114 residues).

In summary, an improved $^{1}H^{N}$-based CPMG pulse scheme is presented for studies of millisecond timescale exchange dynamics in protonated proteins. The

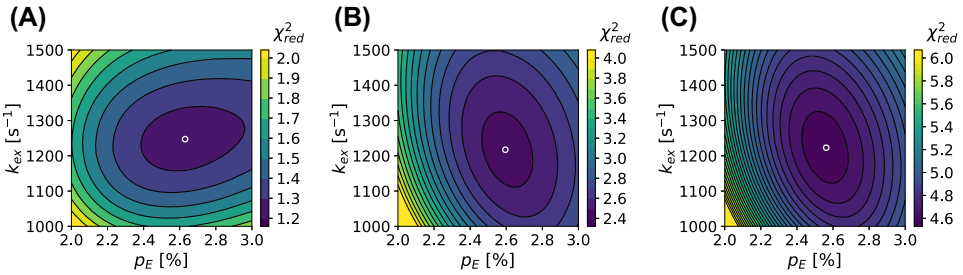

Fig. 6 Reduced χ^2 surface plots of global exchange parameters (p_E, k_{ex}) extracted from fits of ^{15}N (**a**) or $^{1}H^{N}$ (**b**, **c**) dispersion profiles recorded on a fully protonated L99A T4L sample (600 and 800 MHz, 25 °C). In (**b**) and (**c**) the pulse sequences of Figs. 3 and S1 were used, respectively. The position corresponding to the global minimum of χ^2 is indicated by the white circle in each plot

improvement stems from refocusing $^{1}H^{\alpha}$ evolution during the amide proton selective central pulse that leads to flat dispersion profiles in the absence of chemical exchange. Robust chemical exchange parameters and $^{1}H^{N}$ chemical shift differences between probes in the exchanging states are observed for L99A T4L where large dispersion profiles are obtained. Despite the improvements, there are still some limitations with the new approach. For example, the refocusing scheme of Fig. 3 requires that the EBURP pulses selectively excite the amide spins, leaving α-protons unaffected. There may well be outliers in some proteins where this condition is not completely satisfied. In addition, in cases where $\Delta\varpi_{GE}(H^{\alpha}) \neq 0$, incomplete refocusing of $^{1}H^{N}$ magnetization can occur, producing artifacts, Fig. S9. While there remain, therefore, benefits with using highly deuterated samples, it is important to note that high quality $^{1}H^{N}$ dispersion profiles are, in general, produced via the scheme of Fig. 3 using protonated samples, with only slightly higher artifact content in most cases than in corresponding profiles generated from studies with perdeuterated proteins.

Acknowledgements This work was supported by grants from the Canadian Institutes of Health Research (CIHR) and the Natural Sciences and Engineering Research Council of Canada (NSERC) to L.E.K. T.Y. acknowledges post-doctoral support from the CIHR. We thank Pramodh Vallurupalli for useful discussions about exchange dynamics in L99A T4L. L.E.K. holds a Canada Research Chair in Biochemistry.

References

Boehr DD, McElheny D, Dyson HJ, Wright PE (2006) The dynamic energy landscape of dihydrofolate reductase catalysis. Science 313:1638–1642. https://doi.org/10.1126/science.1130258

Bouvignies G, Kay LE (2012) A 2D ^{13}C-CEST experiment for studying slowly exchanging protein systems using methyl probes: an application to protein folding. J Biomol NMR 53:303–310. https://doi.org/10.1007/s10858-012-9640-7

Bouvignies G, Vallurupalli P, Hansen DF, Correia BE, Lange O, Bah A, Vernon RM, Dahlquist FW, Baker D, Kay LE (2011) Solution structure of a minor and transiently formed state of a T4 lysozyme mutant. Nature 477:111–114. https://doi.org/10.1038/nature10349

Bouvignies G, Vallurupalli P, Kay LE (2014) Visualizing side chains of invisible protein conformers by solution NMR. J Mol Biol 426:763–774. https://doi.org/10.1016/j.jmb.2013.10.041

Delaglio F, Grzesiek S, Vuister GW, Zhu G, Pfeifer J, Bax A (1995) NMRPipe: a multidimensional spectral processing system based on Unix pipes. J Biomol NMR 6:277–293. https://doi.org/10.1007/Bf00197809

Dill KA, Chan HS (1997) From Levinthal to pathways to funnels. Nat Struct Biol 4:10–19. https://doi.org/10.1038/nsb0197-10

Dittmer J, Bodenhausen G (2006) Quenching echo modulations in NMR spectroscopy. ChemPhysChem 7:831–836. https://doi.org/10.1002/cphc.200500403

Eriksson AE, Baase WA, Wozniak JA, Matthews BW (1992) A cavity-containing mutant of T4 lysozyme is stabilized by buried benzene. Nature 355:371–373. https://doi.org/10.1038/355371a0

Fawzi NL, Ying JF, Ghirlando R, Torchia DA, Clore GM (2011) Atomic-resolution dynamics on the surface of amyloid-β protofibrils probed by solution NMR. Nature 480:268–272. https://doi.org/10.1038/nature10577

Geen H, Freeman R (1991) Band-selective radiofrequency pulses. J Magn Reson 93:93–141. https://doi.org/10.1016/0022-2364(91)90034-q

Hansen DF, Vallurupalli P, Kay LE (2008a) An improved ^{15}N relaxation dispersion experiment for the measurement of millisecond time-scale dynamics in proteins. J Phys Chem B 112:5898–5904. https://doi.org/10.1021/jp074793o

Hansen DF, Vallurupalli P, Lundström P, Neudecker P, Kay LE (2008b) Probing chemical shifts of invisible states of proteins with relaxation dispersion NMR spectroscopy: How well can we do? J Am Chem Soc 130:2667–2675. https://doi.org/10.1021/ja078337p

Hansen AL, Lundström P, Velyvis A, Kay LE (2012) Quantifying millisecond exchange dynamics in proteins by CPMG relaxation dispersion NMR using side-chain ^{1}H probes. J Am Chem Soc 134:3178–3189. https://doi.org/10.1021/ja210711v

Henzler-Wildman K, Kern D (2007) Dynamic personalities of proteins. Nature 450:964–972. https://doi.org/10.1038/nature06522

Ishima R, Torchia DA (2000) Protein dynamics from NMR. Nat Struct Biol 7:740–743. https://doi.org/10.1038/78963

Ishima R, Torchia DA (2003) Extending the range of amide proton relaxation dispersion experiments in proteins using a constant-time relaxation-compensated CPMG approach. J Biomol NMR 25:243–248. https://doi.org/10.1023/A:1022851228405

Ishima R, Wingfield PT, Stahl SJ, Kaufman JD, Torchia DA (1998) Using amide ^{1}H and ^{15}N transverse relaxation to detect millisecond time-scale motions in perdeuterated proteins: Application to HIV-1 protease. J Am Chem Soc 120:10534–10542. https://doi.org/10.1021/ja981546c

Ishima R, Freedberg DI, Wang YX, Louis JM, Torchia DA (1999) Flap opening and dimer-interface flexibility in the free and inhibitor-bound HIV protease, and their implications for function. Structure 7:1047–1055. https://doi.org/10.1016/S0969-2126(99)80172-5

Ishima R, Baber J, Louis JM, Torchia DA (2004) Carbonyl carbon transverse relaxation dispersion measurements and ms–μs time-scale motion in a protein hydrogen bond network. J Biomol NMR 29:187–198. https://doi.org/10.1023/B:JNMR.0000019249.50306.5d

Jiang B, Yu BH, Zhang X, Liu ML, Yang DW (2015) A ^{15}N CPMG relaxation dispersion experiment more resistant to resonance offset and pulse imperfection. J Magn Reson 257:1–7. https://doi.org/10.1016/j.jmr.2015.05.003

Karplus M, Kuriyan J (2005) Molecular dynamics and protein function. Proc Natl Acad Sci USA 102:6679–6685. https://doi.org/10.1073/pnas.0408930102

Karplus M, McCammon JA (1983) Dynamics of proteins: elements and function. Annu Rev Biochem 52:263–300. https://doi.org/10.1146/annurev.bi.52.070183.001403

Korzhnev DM, Kloiber K, Kanelis V, Tugarinov V, Kay LE (2004a) Probing slow dynamics in high molecular weight proteins by methyl-TROSY NMR spectroscopy: application to a 723-residue enzyme. J Am Chem Soc 126:3964–3973. https://doi.org/10.1021/ja039587i

Korzhnev DM, Salvatella X, Vendruscolo M, Di Nardo AA, Davidson AR, Dobson CM, Kay LE (2004b) Low-populated folding intermediates of Fyn SH3 characterized by relaxation dispersion NMR. Nature 430:586–590. https://doi.org/10.1038/nature02655

Loria JP, Rance M, Palmer AG (1999) A relaxation-compensated Carr–Purcell–Meiboom–Gill sequence for characterizing

chemical exchange by NMR spectroscopy. J Am Chem Soc 121:2331–2332. https://doi.org/10.1021/ja983961a

Lundström P, Hansen DF, Vallurupalli P, Kay LE (2009) Accurate measurement of alpha proton chemical shifts of excited protein states by relaxation dispersion NMR spectroscopy. J Am Chem Soc 131:1915–1926. https://doi.org/10.1021/ja807796a

Marion D, Ikura M, Tschudin R, Bax A (1989) Rapid recording of 2D NMR spectra without phase cycling. Application to the study of hydrogen exchange in proteins. J Magn Reson 85:393–399. https://doi.org/10.1016/0022-2364(89)90152-2

McConnell HM (1958) Reaction rates by nuclear magnetic resonance. J Chem Phys 28:430–431. https://doi.org/10.1063/1.1744152

Mittermaier A, Kay LE (2001) χ_1 torsion angle dynamics in proteins from dipolar couplings. J Am Chem Soc 123:6892–6903. https://doi.org/10.1021/ja010595d

Mittermaier A, Kay LE (2006) New tools provide new insights in NMR studies of protein dynamics. Science 312:224–228. https://doi.org/10.1126/science.1124964

Mulder FAA, Skrynnikov NR, Hon B, Dahlquist FW, Kay LE (2001) Measurement of slow (μs–ms) time scale dynamics in protein side chains by ^{15}N relaxation dispersion NMR spectroscopy: application to Asn and Gln residues in a cavity mutant of T4 lysozyme. J Am Chem Soc 123:967–975. https://doi.org/10.1021/ja003447g

Mulder FAA, Hon B, Mittermaier A, Dahlquist FW, Kay LE (2002) Slow internal dynamics in proteins: application of NMR relaxation dispersion spectroscopy to methyl groups in a cavity mutant of T4 lysozyme. J Am Chem Soc 124:1443–1451. https://doi.org/10.1021/jp0119806

Neudecker P, Robustelli P, Cavalli A, Walsh P, Lundström P, Zarrine-Afsar A, Sharpe S, Vendruscolo M, Kay LE (2012) Structure of an intermediate state in protein folding and aggregation. Science 336:362–366. https://doi.org/10.1126/science.1214203

Palmer AG, Massi F (2006) Characterization of the dynamics of biomacromolecules using rotating-frame spin relaxation NMR spectroscopy. Chem Rev 106:1700–1719. https://doi.org/10.1021/cr0404287

Palmer AG, Kroenke CD, Loria JP (2001) Nuclear magnetic resonance methods for quantifying microsecond-to-millisecond motions in biological macromolecules. Methods Enzymol 339:204–238. https://doi.org/10.1016/S0076-6879(01)39315-1

Sekhar A, Kay LE (2019) An NMR view of protein dynamics in health and disease. Annu Rev Biophys 48:297–319. https://doi.org/10.1146/annurev-biophys-052118-115647

Sekhar A, Rumfeldt JAO, Broom HR, Doyle CM, Bouvignies G, Meiering EM, Kay LE (2015) Thermal fluctuations of immature SOD1 lead to separate folding and misfolding pathways. eLife 4:e07296. https://doi.org/10.7554/elife.07296

Sekhar A, Velyvis A, Zoltsman G, Rosenzweig R, Bouvignies G, Kay LE (2018) Conserved conformational selection mechanism of Hsp70 chaperone-substrate interactions. eLife 7:e32764. https://doi.org/10.7554/elife.32764

Shaka AJ, Keeler J, Frenkiel T, Freeman R (1983) An improved sequence for broadband decoupling: WALTZ-16. J Magn Reson 52:335–338. https://doi.org/10.1016/0022-2364(83)90207-X

Sklenar V, Piotto M, Leppik R, Saudek V (1993) Gradient-tailored water suppression for ^{1}H–^{15}N HSQC experiments optimized to retain full sensitivity. J Magn Reson 102:241–245. https://doi.org/10.1006/jmra.1993.1098

Skrynnikov NR, Mulder FAA, Hon B, Dahlquist FW, Kay LE (2001) Probing slow time scale dynamics at methyl-containing side chains in proteins by relaxation dispersion NMR measurements: application to methionine residues in a cavity mutant of T4 lysozyme. J Am Chem Soc 123:4556–4566. https://doi.org/10.1021/ja004179p

Tollinger M, Skrynnikov NR, Mulder FAA, Forman-Kay JD, Kay LE (2001) Slow dynamics in folded and unfolded states of an SH3 domain. J Am Chem Soc 123:11341–11352. https://doi.org/10.1021/ja011300z

Vallurupalli P, Hansen DF, Stollar E, Meirovitch E, Kay LE (2007) Measurement of bond vector orientations in invisible excited states of proteins. Proc Natl Acad Sci USA 104:18473–18477. https://doi.org/10.1073/pnas.0708296104

Vallurupalli P, Sekhar A, Yuwen T, Kay LE (2017) Probing conformational dynamics in biomolecules via chemical exchange saturation transfer: a primer. J Biomol NMR 67:243–271. https://doi.org/10.1007/s10858-017-0099-4

Yip GNB, Zuiderweg ERP (2004) A phase cycle scheme that significantly suppresses offset-dependent artifacts in the R_2-CPMG ^{15}N relaxation experiment. J Magn Reson 171:25–36. https://doi.org/10.1016/j.jmr.2004.06.021

Yuwen T, Skrynnikov NR (2014) Proton-decoupled CPMG: a better experiment for measuring ^{15}N R_2 relaxation in disordered proteins. J Magn Reson 241:155–169. https://doi.org/10.1016/j.jmr.2013.08.008

Yuwen T, Vallurupalli P, Kay LE (2016) Enhancing the sensitivity of CPMG relaxation dispersion to conformational exchange processes by multiple-quantum spectroscopy. Angew Chem Int Ed 55:11490–11494. https://doi.org/10.1002/anie.201605843

Yuwen T, Huang R, Vallurupalli P, Kay LE (2019) A methyl-TROSY-based ^{1}H relaxation dispersion experiment for studies of conformational exchange in high molecular weight proteins. Angew Chem Int Ed 58:6250–6254. https://doi.org/10.1002/anie.201900241